

Symmetrized splitting operator method for dynamic consolidation problem of saturated porous semi-infinite foundation

Huaifa Ma^{a,b,1}, Yifu Song^{c,1,*}, Changgen Bu^{d,**}, Yusheng Yang^a

^a State Key Laboratory of Simulation and Regulation of Water Cycle in River Basin, China Institute of Water Resources and Hydropower Research, Beijing, 100048, PR China

^b Earthquake Engineering Research Center, China Institute of Water Resources and Hydropower Research, Beijing, 100048, PR China

^c Key Laboratory of Computational Geodynamics, University of Chinese Academy of Sciences, Beijing, 100049, PR China

^d School of Engineering and Technology, China University of Geosciences, Beijing, 100083, PR China

ARTICLE INFO

Keywords:

Finite element method
Dynamic consolidation
Splitting operator method
Pore water pressure
Viscous-spring boundary

ABSTRACT

The u - p form of dynamic consolidation equation provides a convenient approach to get insights into lots of low frequency practical engineering problems. Since the coupling of the dynamic consolidation equation, the existing numerical methods are generally full-implicit or staggered implicit which are always time-consuming. As a motivation to give a fast numerical algorithm for multi-field coupling problems, we construct a symmetrized splitting method in this paper to solve the u - p dynamic consolidation equations and lead to a second-order explicit scheme. To eliminate the reflection of the artificial boundary waves, we have derived the flow conditions of the artificial visco-spring boundary (VSB) for semi-infinite 3D saturated foundations, and presented principle for virtual displacements of the dynamic consolidation problem with artificial VSBs. Furthermore, we take the VSB condition of the fluid-solid two-phase saturated medium into consideration, to simulate the dynamic response process of saturated porous semi-infinite foundation system. The high computational efficiency and stability of the proposed method are verified by the numerical experiments.

1. Introduction

Saturated soil, a typical two-phase porous medium composed of pore fluid (pore water) and soil skeleton, is commonly referred to as a saturated porous medium. The relationship between pore pressure dissipation and soil skeleton deformation can be accurately described by Biot's consolidation theory [1]. Denote by u the solid skeleton displacement, U the fluid displacement, w the relative fluid displacement, and p the pore pressure in the fluid. By the Biot's consolidation theory, different consolidation problems come down to the u - U , u - w or u - p forms of equations [2–4]. The u - p form of dynamic consolidation equation shows valid for most low frequency engineering problems [2]. Therefore, it is often used as a standard approach when solving consolidation equations numerically. The soil skeleton displacement u and the pore water pressure p are the essential physical variables of soil liquefaction problem and can be directly obtained by solving the u - p form of consolidation equations.

Traditionally, the coupling dynamic responses of the solid and

liquid phases in a saturated two-phase medium is solved by treating the entire system as a computational entity and all field state variables are simultaneously advanced in time (direct time integration procedures) [5]. Although the matrices on the diagonals in the spatial semi-discrete systems of the u - p equations are symmetric, the overall matrices are not. Since the simultaneous implicit procedures involve unacceptable computational costs, the staggered solution procedures came into being. In such procedures, the solution state of the coupled system is advanced by sequentially executing the subsystem analyzers [6]. Further, Park [7] applied the matrix augmentation concept in a fluid-structure interaction problem, and recommended a staggered implicit-implicit procedure, which was further improved to unconditionally stable procedure by Zienkiewicz et al. [8,9]. For implicit simultaneous solution procedure, enormous local bandwidths would appear in the resulting coefficient matrices, and assembling and solving equations is required. Although the staggered implicit procedure can sequentially decouple a single physics, it also requires assembling and solving equations of each subsystem, and its computational efficiency per time step is

* Corresponding author.

** Corresponding author.

E-mail addresses: mahf@iwhr.com (H. Ma), songyifu16@mails.ucas.edu.cn (Y. Song), bucg@cugb.edu.cn (C. Bu).

¹ H. Ma and Y. Song contributed equally.

counteracted by the fact that satisfactory numerical stability properties may be hard to achieve.

Moreover, no matter the simultaneous implicit procedures or the staggered procedures, the so-called Babuška-Brezzi (BB) conditions [10–13] need to be satisfied in the limit of nearly incompressible pore fluid and small permeability, since the matrix coefficients of the (u, u) subsystem would be much larger than that of the (p, p) subsystem in such cases. The BB conditions pose severe restrictions on the use of interpolation functions for u and p in the finite element discretization. To avoid such restrictions, one could resort to mixed finite element methods (higher order for u , lower order for p) for stress-displacement formulations [14,15] or use time-stepping schemes to solve incompressible problems directly for steady state or iteratively through the time domain [16–18]. These approaches sometimes complicate coding and result in inconvenient forms or uneconomical small time steps.

Taking into account both the computing efficiency and the stability criteria, the practical feasibility of an approach mainly hinges upon the performance of solving large-scale coupling problems and the stability of the time integration procedure. In this paper, we seek the splitting operator method for help, which can effectively avoid the disadvantages of the couple methodology and the restrictions of BB conditions. That is our motivation to develop a high-performance and fully explicit algorithm to solve the long-term consolidation problems of soil foundation and soil liquefaction under earthquake.

The basic principle of the splitting operator method is to split the original system into a set of simpler sub-systems and devise a strategy that alternates between solving these sub-systems in certain sequence, which is then approximate to the solution of full system to a certain order of accuracy. Since the split divide the equations in parts that are solved in different time steps, such methods are also called time splitting methods or fractional methods. For a more detailed review of splitting methods one can refer [19].

The idea of splitting approach was first proposed by Trotter in the 1950s, who give an approximation of order one, named the Lie-Trotter splitting, to the solution of ordinary differential problems. Such method was first applied to partial differential systems [20]. Strang splitting [21] is another famous and important splitting approach which was introduced by Strang in 1963. This approach, also called the symmetrized splitting operator method, can achieve second-order accuracy by a symmetrized composition of the Lie-Trotter method and its adjoint with halved step size. There are also efforts to construct higher order splitting methods or design other two-order precision splitting methods, such as the method of Yasuo [22]. However, most of them are not widely used or might be only suitable for some fixed schemes. In the past few decades, the splitting approaches have been successfully applied to solve complex partial differential equations and practical problems. Zeng et al. applied the splitting methods in solving the equations of atmospheric motion [23,24], since the separability of the fast stage and the slow and good time effects can be obtained. Among the splitting approaches, the Strang splitting is one of the most used method. There are lots of studies about its application, such as the convection-diffusion problems [25], Navier-Stokes equations [26], the turbulence and interface problems [27], Benjamin-Bona-Mahony type equations [28], and the Vlasov-Maxwell (VM) system [29,30]. For some detailed models and situations, the classic splitting scheme can not use directly or may lose some good properties, such as the symmetrical characteristic for the Strang splitting method. Thus there are also many researches have been done to make modifications or construct improved method [31,32]. As far as we known, the operator splitting methods has not yet been used to solve the u - p form of dynamic consolidation equation. Thus we seek the help of splitting algorithms here and develop the symmetric splitting operator method (SSOM) for the dynamic consolidation equations of saturated porous media.

Furthermore, the artificial boundary is considered in our research. In the dynamic analysis of the finite element method, the semi-infinite

foundation is generally divided into the near-field foundation of the adjacent structure and far-field foundation of its periphery. To correctly describe the wave propagation at infinity, the radiation damping of unbounded domain must be modeled accurately. In the past 40 years, a lot of research effort has been contributed to the artificial boundary [33–37]. At present, what is mainly applied is the artificial transmitting boundary [33], viscous boundary [34], and viscous-spring boundary (VSB) [35–37]. In recent years, the scaled boundary finite element method (SBFEM) [38–40] has been applied to solve the problem of time dependence in unbounded domains. But at present, SBFEM can only be used to solve some simple 2D problems. The VSB is added with springs on the basis of the viscous boundary, which absorb the wave energies radiating to the artificial boundaries by means of setting simple mechanical models consisting of a series of linear springs and dampers in order to eliminate reflection, and to simulate the elastic recovery capability of the foundation, as well as potentially effectively simulating the true spread process of the waves in an infinite foundation. And VSB is widely used because it is simple in expression and easy to apply to complex conditions.

However, different from the artificial boundary of the single phase solid structure mentioned above, it is necessary to consider the displacement boundary conditions on the artificial boundary of the saturated soil, and also consider the diffusion of pore water pressure. Based on the simplified Biot's equation, Modaressi et al. [41] proposed the viscous boundary of the u - p form of the saturated medium dynamic equation. Akiyoshi et al. [42] also investigated the viscous boundaries of saturated media in the form of u - w and u - U . Liu and Song [43] putted forward 2D VSBs of the saturated foundation based on a cylindrical wave for the u - p form of 2D dynamic consolidation problem. However, the artificial VSBs for the 3D problem are rarely investigated.

In this paper, we will present the flow conditions of the 3D artificial VSB for the u - p equations of dynamic consolidation problem of saturated porous semi-infinite foundation, and establish the unified virtual displacement principle of 3D saturated medium dynamic consolidation problem with artificial VSB. Combining SSOM with the VSB of a fluid-solid two-phase saturated medium to absorb outgoing waves, we will simulate the dynamic consolidation processes of saturated porous semi-infinite foundation.

The rest of the article is organized as follows. In Section 2, the construction of symmetrized splitting operator method for dynamic consolidation equations is introduced. In Section 3, the numerical analysis is executed to verify the split operator formats, the numerical stability and the computational efficiency. Section 4 illustrates the SSOM that introduces the VSB and its energy absorption effect. Finally, Section 5 presents concluding remarks.

2. SSOM for dynamic consolidation equations

2.1. Dynamic consolidation equation and its boundary conditions

In case of medium-low frequency and seismic effect analysis, the acceleration terms of fluid are neglected, the simplified dynamic consolidation equations [2] is given as

$$\sigma'_{ij} + \alpha \delta_{ij} p_i + \rho \ddot{u}_i = \rho b_i \quad (1a)$$

$$k_f p_{ii} + \alpha \dot{\epsilon}_{ii} - \frac{1}{Q} \dot{p} = 0 \quad (1b)$$

where $i, j = 1, 2, 3$, and the Einstein's summation convention is used, which assumed that the compressive stress in saturated media is positive, and tensile stress is negative.

2.1.1. Definitions of the parameters

σ_{ij} : the total stress of the saturated media, σ'_{ij} : the effective stress, p : the pressure of pore fluid (water);

u_i : the displacement, \ddot{u}_i : the acceleration, $\varepsilon_{ij} = (u_{i,j} + u_{j,i})/2$: the strain, $\dot{\varepsilon}_{ii}$: the volumetric strain rate of the solid skeleton;
 $\rho = (1 - n)\rho_s + n\rho_f$: the density of saturated media, ρ_s, ρ_f : the densities of the solid and fluid phases, respectively, b : the acceleration of the mixture gravity;
 k_f : the dynamic permeability coefficient, γ_w : the bulk density of water, k : the permeability coefficient with the relationship $k_f = k/\gamma_w$;
 λ, μ : the Lamé constant of the solid skeleton;

$\alpha = 1 - K_b/K_s, Q = 1/[n/K_f + (\alpha - n)/K_s]$: the related coefficients of compressibility of solid and fluid, where K_s, K_f and $K_b = \lambda + 2\mu/3$ are the bulk modulus of solid particles, fluids and solid skeletons, respectively.

In the effective stress analysis of saturated porous media dynamic consolidation, there are four boundaries:

- (1) Displacement boundary Γ_u : $u = u_0, v = v_0$
- (2) Stress boundary Γ_σ : $-(\sigma_{ij} - p\delta_{ij})n_j = T_i, -\sigma'_{ij}n_j = T'_i$
- (3) Porous pressure boundary Γ_p : $p = p_0$
- (4) Flux boundary Γ_q : $q_n = -k_f p_i n_i$

Taking the inner product of equations (1a) and (1b) with the virtual displacement δu_i and the pressure δp respectively, system (1) then comes to the following weak formulations under the above boundary conditions:

$$\left\{ \begin{aligned} & \int_{\Omega} \ddot{u} \delta u_i d\Omega + \int_{\Omega} \rho \ddot{u}_i \delta u_i d\Omega + \int_{\Gamma_u} T_i \delta u_i d\Gamma + \int_{\Omega} \alpha p \delta \varepsilon_{ii} d\Omega + \int_{\Gamma_p} \alpha p n_i \delta u_i d\Gamma \\ & = 0 \\ & \int_{\Omega} \frac{1}{Q} \dot{p} \delta p d\Omega + \int_{\Omega} k_f p_i \delta p_i d\Omega + \int_{\Gamma_q} q_n \delta p d\Gamma - \int_{\Omega} \alpha \dot{\varepsilon}_{ii} \delta p d\Omega = 0 \end{aligned} \right. \quad (2)$$

After applying the finite element discretization to Eq. (2), we can immediately obtain an ordinary differential equations with respect to time:

$$\begin{cases} A\ddot{\mathbf{u}} + B\dot{\mathbf{u}} + C\mathbf{p} = 0 \\ D\dot{\mathbf{p}} + E\mathbf{p} - F\dot{\mathbf{u}} = 0 \end{cases} \quad (3)$$

where A, B, C, D, E and F are coefficient matrices containing the discrete terms of the boundary conditions, $\ddot{\mathbf{u}}, \dot{\mathbf{u}}, \mathbf{u}$ and \mathbf{p} are the node vectors of solid skeleton acceleration, velocity, displacement and pore water pressure, respectively.

2.2. Splitting operator scheme for dynamic consolidation equations

This subsection is devoted to the construction of SSOM for the u - p manner of the dynamic consolidation equation of the two-phase saturated medium.

First, we introduce a new parameter \mathbf{v} defined as $\mathbf{v} = \dot{\mathbf{u}}$, which is actually velocity vector. Thus, the second order ordinary differential system, obtained by spatial discretization, can be rewritten as the following first order system.

$$\begin{cases} \dot{\mathbf{u}} = \mathbf{v}, \\ \dot{\mathbf{v}} = -A^{-1}B\mathbf{u} - A^{-1}C\mathbf{p}, \\ \dot{\mathbf{p}} = -D^{-1}E\mathbf{p} + D^{-1}F\mathbf{v}. \end{cases} \quad (4)$$

According to the principle of the splitting algorithm, the vector field of system (4) can be decomposed into three sub-systems of variable \mathbf{u}, \mathbf{v} and \mathbf{p} , which can be explicitly and separately calculated.

- (1) The subsystem associated with the displacement \mathbf{u} is equivalent to

$$\varphi^u(\Delta t): \begin{cases} \dot{\mathbf{u}} = 0, \\ \dot{\mathbf{v}} = -A^{-1}B\mathbf{u}, \\ \dot{\mathbf{p}} = 0. \end{cases} \quad (5a)$$

The exact update mapping of the subsystem $\varphi^u(\Delta t)$ with step size Δt is

$$\begin{cases} \mathbf{u}(t + \Delta t) = \mathbf{u}(t) \\ \mathbf{v}(t + \Delta t) = \mathbf{v}(t) - \Delta t A^{-1} B \mathbf{u}(t) \\ \mathbf{p}(t + \Delta t) = \mathbf{p}(t) \end{cases} \quad (5b)$$

- (2) The subsystem associated with the velocity \mathbf{v} is equivalent to

$$\varphi^v(\Delta t): \begin{cases} \dot{\mathbf{u}} = \mathbf{v}, \\ \dot{\mathbf{v}} = 0, \\ \dot{\mathbf{p}} = -D^{-1}E\mathbf{p}. \end{cases} \quad (6a)$$

The exact mapping update of the subsystem $\varphi^v(\Delta t)$ with step size Δt is

$$\begin{cases} \mathbf{u}(t + \Delta t) = \mathbf{u}(t) + \Delta t \mathbf{v}(t), \\ \mathbf{v}(t + \Delta t) = \mathbf{v}(t), \\ \mathbf{p}(t + \Delta t) = \mathbf{p}(t) + \Delta t D^{-1} E \mathbf{v}(t). \end{cases} \quad (6b)$$

- (3) The subsystem associated with the pore water pressure p is equivalent to

$$\varphi^p(\Delta t): \begin{cases} \dot{\mathbf{u}} = 0, \\ \dot{\mathbf{v}} = -A^{-1}C\mathbf{p}, \\ \dot{\mathbf{p}} = -D^{-1}E\mathbf{p}. \end{cases} \quad (7a)$$

The exact mapping update of the subsystem $\varphi^p(\Delta t)$ with step size Δt is

$$\begin{cases} \mathbf{u}(t + \Delta t) = \mathbf{u}(t), \\ \mathbf{v}(t + \Delta t) = \mathbf{v}(t) - \Delta t A^{-1} C \mathbf{p}(t), \\ \mathbf{p}(t + \Delta t) = \mathbf{p}(t) - \Delta t D^{-1} E \mathbf{p}(t). \end{cases} \quad (7b)$$

By using the technique of composition method, the first-order methods (5b), (6b), (7b) with halved time step sizes and their adjoint methods can be composed to get a symmetric second order scheme, i.e. the symmetrized splitting operator method (SSOM):

$$\Phi(\Delta t) = \varphi_1^u(\Delta t/2) \circ \varphi_2^v(\Delta t/2) \circ \varphi_3^p(\Delta t) \circ \varphi_4^v(\Delta t/2) \circ \varphi_5^u(\Delta t/2) \quad (8)$$

Finally, the displacement \mathbf{u} and pore water pressure p of the saturated medium can be obtained by solving the full-discrete system (8).

The decomposed steps of SSOM can be depicted in Fig. 1.

3. Numerical analysis verification for SSOM

3.1. Numerical example of dynamic consolidation of a saturated soil column

To verify the effectiveness and practicability of splitting operator scheme, a numerical model of the dynamic consolidation is shown in Fig. 2. Here the dynamic responses under sudden loading are executed.

The origin of coordinate system is located in the left corner of the bottom surface of the model. The cube is $3\text{ m} \times 3\text{ m} \times 30\text{ m}$, and the surface load is applied to the upper surface which is water-permeable and the normal displacement free; the surrounding and bottom surfaces are impermeable, and the normal displacements are constrained. For comparative analysis, the material parameters are listed in Table 1, which are consistent with those of Zienkiewicz et al. [2,8]. The finite element mesh is regular hexahedron with a size of $3\text{ m} \times 3\text{ m} \times 3\text{ m}$.

The load time history is shown in Fig. 2(b) whose peak value is 1 kPa. The initial pore pressure is equal to 1 kPa, while initial velocity and initial displacement are assumed to be zero. Take the time step $\Delta T = 0.004\text{ s}$, and the calculation lasts for 30s.

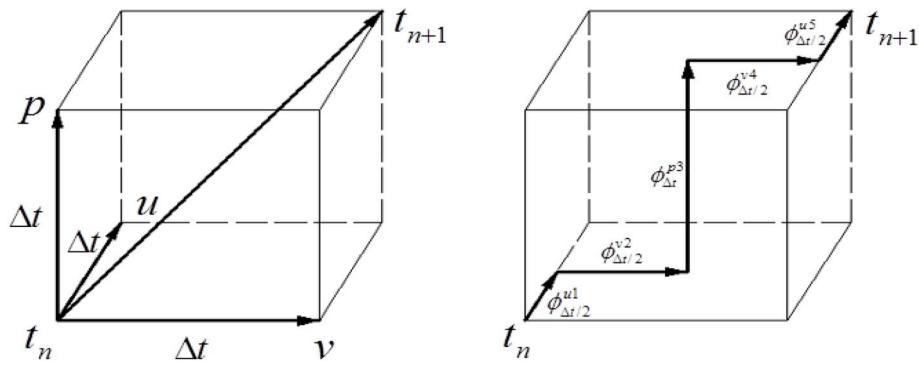


Fig. 1. Decomposition of vector in the splitting operator method.

The calculated time history curves of the pore water pressure and the calculated displacement time histories at three different points A (0,0,27), B (0,0,15), C (0,0,3) are selected, which are listed in Fig. 3. The pressure of pore water time history indicated by the legends (a), (b), and (c) is the (one-dimensional analytical solution) theoretical curve [2]. The calculation results are indicated by the legends (A), (B) and (C). As can be seen from Fig. 3(a), the calculated pore water pressure curves are almost identical to the theoretical solution. At A (0,0,27), B (0,0,15), and C (0,0,3) points, the calculated displacement time histories are shown in Fig. 3(b), which are basically consistent with that of one-dimensional numerical model, calculated by Zienkiewicz et al. [8]. This numerical analysis leads us to conclude that the proposed SSOM is correct and valid.

3.2. Numerical stability of the symmetrized splitting operator method

The second order explicit scheme derived from SSOM avoids the complex problem of solving the matrix inversion of the simultaneous equations. Generally, explicit formation requires a smaller computer memory, the programming is relatively simple, and the calculation process is easy to implement. To achieve the stability, the calculation time step must be less than the critical time step, determined by the highest natural frequency of the system.

According to the element size, material and mechanical property parameters, the propagation speeds of the compressive wave, and the shear wave can be calculated as $V_p = 464.4m/s$, and $V_s = 85.75m/s$, respectively. Theoretically, the time interval is $DT \leq \Delta t_{cr} = L/V_p = 3.0/464.4 = 0.0065s$. Based on the above calculation and analysis, a series of stability analyses can be performed with additional time intervals of 0.003s, 0.005s, 0.006s, 0.008s and $\geq 0.01s$,

Table 1
Material properties from numerical examples.

Material Parameters	Symbol	Value
Bulk modulus of solid	K_s	100 GPa
Bulk modulus of pore fluid	K_f	100 MPa
Density of pore fluid	ρ_f	$10^3 kg/m^3$
Mass density of solid	ρ_s	$2 \times 10^3 kg/m^3$
Porosity	n	0.3
Poisson ratio	ν	0.2
Young modulus	E	30.0 MPa
Permeability	k	$10^{-2} kg/m$

respectively. The calculations of first four time increment steps are stable, but divergent at the time intervals of greater than 0.01s. Although, 0.008s is slightly larger than the theoretical stability interval, its calculation is still stable. The above analysis indicates that a simple rough estimate of the stabilization time interval is still substantially effective.

In the stable calculation, the pressure of pore water versus time histories of the points C (0,0,3) and the displacement time histories of the point A (0,0,27) are shown in Fig. 4(a) and 4(b), separately.

The relative errors between calculated values and Theoretical reference values (Zienkiewicz et al. [8]) of the pore pressure and the displacement at 30s by different time steps are shown in Table 2. Results and analyses of these Figures and Tables lead us to confirm that the calculation results of different time increments are basically consistent with the theoretical or reference curves, either the evolution of pore water pressure or the change of displacement. It can be seen that when the time interval DT takes 0.004 s, the calculation result of the

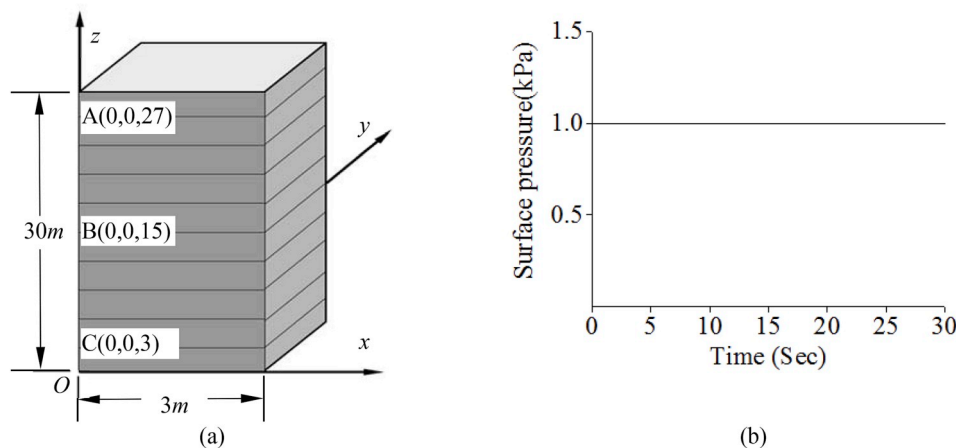


Fig. 2. The dynamic consolidation of a saturated soil column: (a) Finite element model; (b) Loading process.

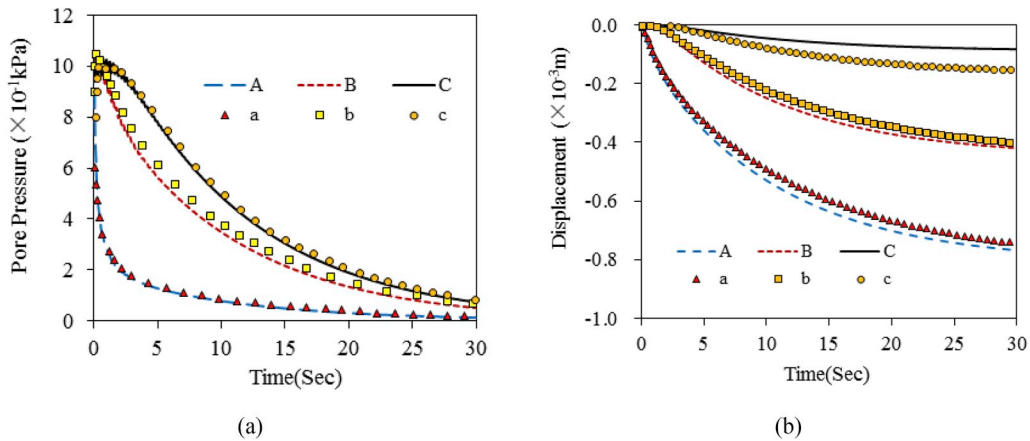


Fig. 3. Comparison between the calculation results of SSOM and analytical solution: (a) Time histories of the pore pressure; (b) Time histories of the displacement.

pore pressure is closer to the theoretical solution, the relative error is 10.13%, while the relative error of the vertical displacement is only 3.69%. Thus we chose $DT = 0.004s$ in the following experiments after comprehensive consideration.

To prepare for the next section to discuss computational efficiency of SSOM, in Appendix I, we briefly introduce the construction of traditionally implicit scheme of the $u-p$ system. The dynamic displacement equation and the pore pressure diffusion equation are discretized in an implicit format Eq. (A1.3) and solved simultaneously with a time interval of $0.004s$. The calculation results at Point A, Point B and Point C by using the Implicit scheme (IM) can be seen in Fig. 5, which are completely consistent with the results obtained by using SSOM.

3.3. Computational efficiency of SSOM

In this section, the good computational efficiency of our proposed explicit method is verified through some numerical calculations. To make comparison, an implicit approach Eq. (A1.3) is also used here to solve the dynamic consolidation problem of the model shown in Fig. 6. The model size is $48\text{ m} \times 48\text{ m} \times 24\text{ m}$, where the upper part is a free drainage surface, and the surface load is added on the area of $8\text{ m} \times 8\text{ m}$ at the center of the upper surface. The surface loading history shown in Fig. 2 is still used. The bottom surface and the four sides are set to be impervious and a normal displacement constraint is applied.

The minimum mesh size of finite element calculation is

$2\text{ m} \times 2\text{ m} \times 2\text{ m}$ for regular hexahedron, as shown in Fig. 6(b). There are altogether 2601 nodes and 2048 hexahedron elements, 7803° of freedom (DOFs) for the whole example concerned. The loading time is taken as 15s. For SSOM, the time step DT ($\leq \Delta_{cr} = L/V_p = 2.0/464.4 = 0.0043s$, the critical time interval) takes $0.004s$. For IM, the multifrontal solver is used, and the time step is taken as $0.004s$, $0.006s$ and $0.008s$, respectively. The computer is configured as Intel(R) Core(TM) i7-5500U@2.4GHz, RAM 8.00 GB.

Table 3 shows the computing times of SSOM and IM with different time steps. One can see that the calculation consuming time of implicit computation is twice more than that of SSOM when $DT = 0.004s$. And the time history curves of the pore water pressure and the displacement time histories at the point A (0,0,22), B (0,20,22) and C (0,24,22) are all compared in Fig. 7. The calculation results show that the pore water pressure and the displacement by using SSOM and IM tend to be consistent. Although by taking larger time interval, the time consuming of IM can be significantly reduced, the oscillation amplitudes of the calculated results would also increase. This situation would be quite severe when DT takes more than $0.01s$. Considering both the calculating time and computational accuracy, SSOM could be a better choice than IM, especially for large-scale computing.

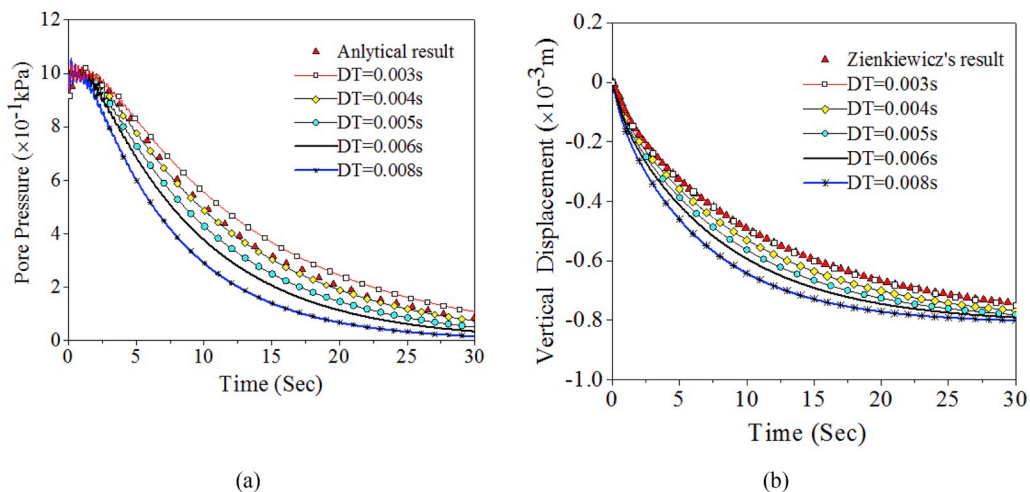


Fig. 4. Stability analysis of SSOM: (a) Pore pressure time history at point C at different time increments; (b) Vertical displacement time history at point A at different time increments.

Table 2
Calculation results by different time intervals loading end to 30s.

Time interval		0.003s	0.004s	0.005s	0.006s	0.008s	Theoretical reference value
Pore pressure	Calculated value (Pa)	107.60	73.22	49.80	33.85	15.61	81.47
	Relative error (%)	32.07	10.13	38.88	58.45	80.84	0.00
Displacement	Calculated value (mm)	-0.75	-0.77	-0.78	-0.79	-0.80	-0.74
	Relative error (%)	1.03	3.69	5.50	6.73	8.15	0.00

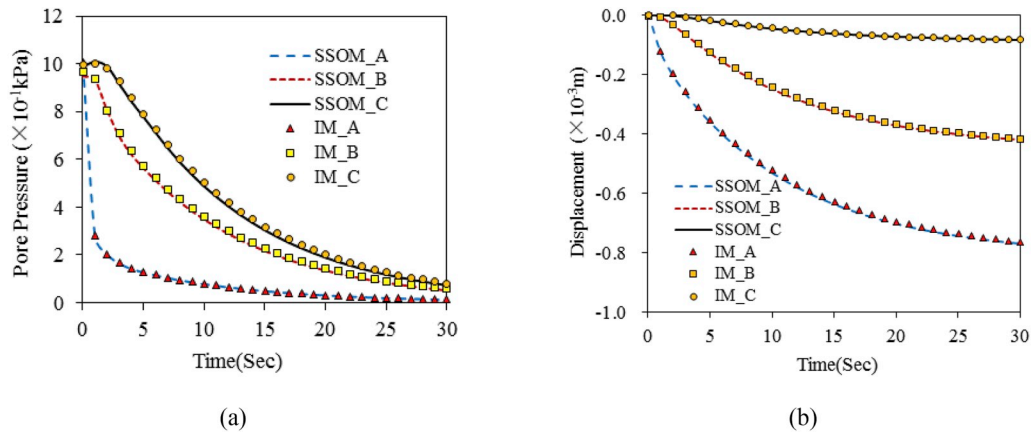


Fig. 5. Comparison between the calculation results of SSOM and IM at Point A, Point B and Point C, respectively: (a)The pore pressure; (b) The displacement.

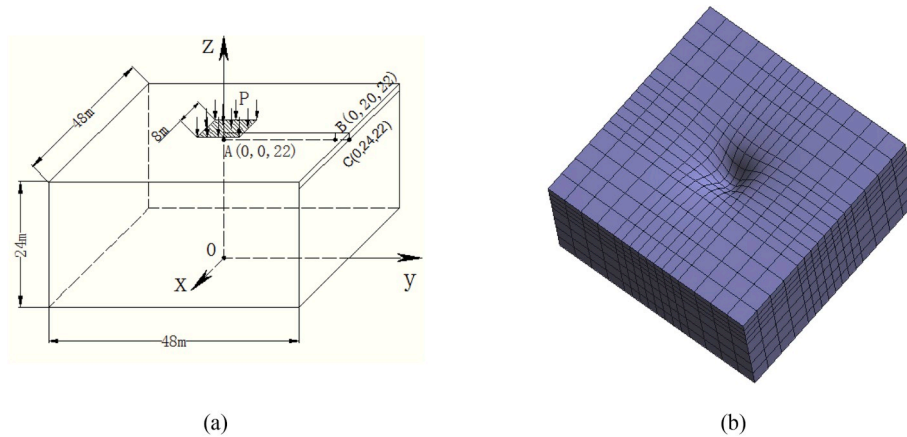


Fig. 6. A numerical model to verify computational efficiency:(a) Dynamic loading model; (b) Finite element mesh (after loaded).

4. SSOM for solving the dynamic consolidation problem of saturated porous semi-infinite foundation

4.1. Artificial VSB model of saturated porous semi-infinite foundation

As shown in Fig. 8, a cubic foundation block is taken from the infinite domain which forms an artificial boundary. The artificial boundary has four sides and a bottom surface. The VSB is employed to simulate the damping effect of the truncated portion.

The displacement wave and the pressure of pore water wave are transmitted on the artificial boundary of the two-phase saturated medium. We have found that the normal and tangential conditions on the VSB of the displacement of the solid skeleton are similar to that of single-phase solid medium [37]. Therefore, we will discuss in detail the water pressure or flow boundary conditions in the normal direction (*vide infra*).

Table 3
Consuming time for different calculation methods loading end to 15s.

Method	SSOM	Implicit algorithm		
Time interval	0.004s	0.004s	0.006s	0.008s
Consumed time	5 h 12min	11 h 52min	6 h 26min	5 h 08min

4.2. Flow conditions of the normal viscoelastic boundary

It is assumed that the source of the scattered wave (in the system) propagates towards the artificial boundary in the form of spherical fluctuations. The radial displacement $u_r \neq 0$ is due to symmetry problem. After ignoring the fluid acceleration and the soil skeleton acceleration, the continuous equation of seepage in the spherical coordinate system is presented as:

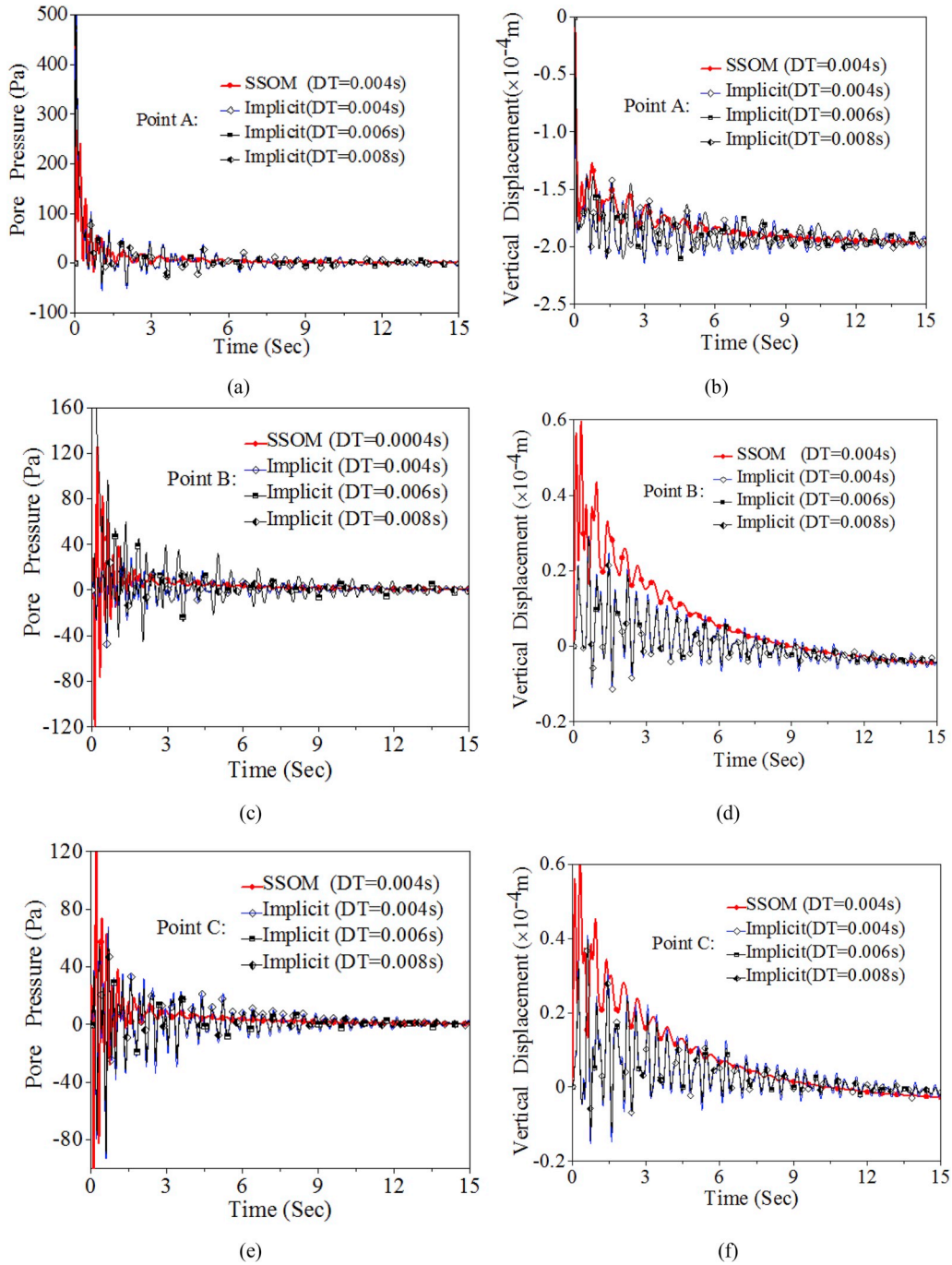


Fig. 7. Comparison between the calculation results of the implicit and explicit algorithm: Time histories of the pore pressure presented in the left column: (a) at point A, (c) at Point B, and (e) at Point C; Displacement responses presented in the right column: (b) at point A, (d) at Point B, and (f) at Point C.

$$k_f \frac{\partial^2 p}{\partial r^2} = \alpha \left(\frac{\partial^2 u_r}{\partial r \partial t} + \frac{2}{r} \frac{\partial u_r}{\partial t} \right) + \frac{1}{Q} \frac{\partial p}{\partial t} \quad (9)$$

When the permeability coefficient k_f is relatively small, taking $k_f = 0$, the error of this assumption is negligible [2]. Thus, Eq. (9) can be expressed as:

$$p = -\alpha Q \left(\frac{\partial u_r}{\partial r} + \frac{2u_r}{r} \right) \quad (10)$$

In the actual mid-low frequency of dynamics engineering, it is assumed that the seepage process of pore water in saturated soil conforms to Darcy's law. Accordingly, the boundary flow in saturated soil medium is expressed as

$$q_r = -k_f \frac{\partial p}{\partial r} \quad (11)$$

If we introduce the displacement potential function $u_r = \partial \varphi / \partial r$, substitute Eq. (10) of the pore water pressure into Eq. (11), then the flow function becomes

$$q_r = \alpha k_f Q \frac{\partial}{\partial r} \left(\frac{\partial^2 \varphi}{\partial r^2} + \frac{2}{r} \frac{\partial \varphi}{\partial r} \right) \quad (12)$$

The spherical wave equation of a 3D saturated medium can be expressed by the potential function φ

$$\frac{\partial^2 \varphi}{\partial t^2} = V_p^2 \left(\frac{\partial^2 \varphi}{\partial r^2} + \frac{2}{r} \frac{\partial \varphi}{\partial r} \right) \quad (13)$$

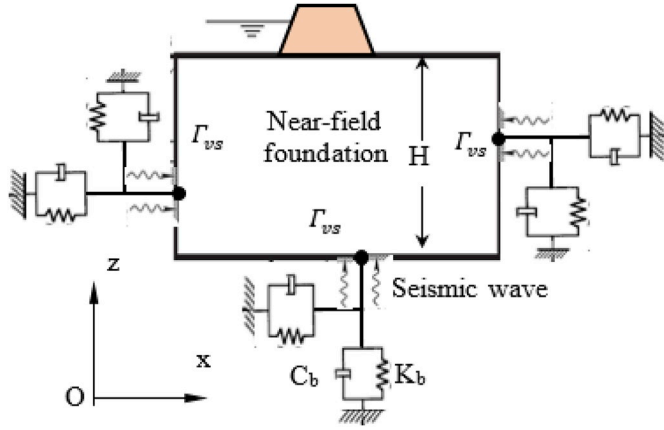


Fig. 8. Artificial VSB model.

Where $V_p = \sqrt{(\lambda + 2\mu + \alpha^2 Q)/\rho}$. It is worth noting that the velocity of the longitudinal wave is different from that of the single-phase solid medium.

By combining Eq. (12) with (13), the boundary normal flow expression is obtained:

$$q_r = \frac{\alpha k_f Q}{V_p^2} \frac{\partial^2}{\partial t^2} \frac{\partial \varphi}{\partial r} = \frac{\alpha k_f Q}{V_p^2} \ddot{u}_r \quad (14)$$

Thus, the normal pressure boundary condition of the artificial boundary is converted into a flow boundary condition, and the boundary normal flow is expressed by the deformation acceleration of the soil skeleton. It can be seen from Eq. (14) that although the 3D wave theory and the governing equation form are different from the 2D, the flux boundary condition on the VSB has the same 2D expression [43].

4.3. Principle of virtual displacement for dynamic consolidation equations with VSB

Since the scattering source is uncertain at a specific location near the field, thus every point of the VSB is on the wave front at a certain scattering point source. Based on the above reasons, the normal flow boundary and the relation of skeleton displacement acceleration can be approximated by Eq. (14), which is $q_n = \frac{\alpha k_f Q}{V_p^2} \ddot{u}_n$.

After introducing the above VSBs, the 3D dynamic consolidation control equations of saturated semi-infinite foundation can be written in the form of virtual work, which is called the principle of virtual displacement for dynamic consolidation equations, as follows:

$$\int_{\Omega} (\sigma'_{ij} \delta \varepsilon_{ij} + \alpha p \delta \varepsilon_{ii}) d\Omega + \int_{\Omega} \rho \ddot{u}_i \delta u_i d\Omega - \int_{\Omega} k_f p_i \delta p_i d\Omega + \int_{\Omega} \alpha \dot{\varepsilon}_{ii} \delta p d\Omega - \int_{\Omega} \frac{1}{Q} \dot{p} \delta p d\Omega$$

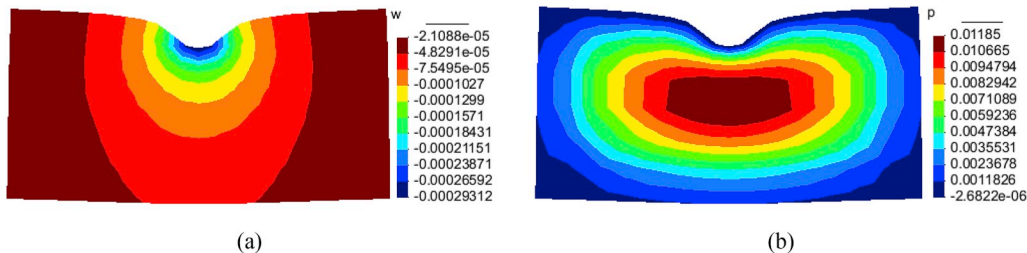


Fig. 9. The calculated results by SSOM with VSB: The cloud diagram of (a) the vertical displacement (m) in the Z-direction, and (b) pore pressure (Pa) on the symmetrical section, respectively.

$$\begin{aligned} + \int_{\Gamma_{vs}} (k_{bij}^m u_j + c_{bij}^m \dot{u}_j) \delta u_i d\Gamma_{vs}^m &= \int_{\Omega} \rho b_i \delta u_i d\Omega + \int_{\Gamma_c} T'_i \delta u_i d\Gamma \\ &- \int_{\Gamma_p} \alpha p n_i \delta u_i d\Gamma + \int_{\Gamma_q \cup \Gamma_{vs}} q_n \delta p d\Gamma \end{aligned} \quad (15)$$

In the above formula, the upper scripts: $m = \pm x, \pm y, -z$, the lower scripts: $i, j, k, l = 1, 2, 3$. Where $q_n = \frac{\alpha k_f Q}{V_p^2} \ddot{u}_n$;

$$[k_b^{\pm x}] = \begin{bmatrix} \frac{E}{2r_b} & 0 & 0 \\ 0 & \frac{G}{2r_b} & 0 \\ 0 & 0 & \frac{G}{2r_b} \end{bmatrix} \quad [c_b^{\pm x}] = \begin{bmatrix} \rho V_p & 0 & 0 \\ 0 & \rho V_s & 0 \\ 0 & 0 & \rho V_s \end{bmatrix}$$

$$[k_b^{\pm y}] = \begin{bmatrix} \frac{G}{2r_b} & 0 & 0 \\ 0 & \frac{E}{2r_b} & 0 \\ 0 & 0 & \frac{G}{2r_b} \end{bmatrix} \quad [c_b^{\pm y}] = \begin{bmatrix} \rho V_s & 0 & 0 \\ 0 & \rho V_p & 0 \\ 0 & 0 & \rho V_s \end{bmatrix}$$

Γ^{vs} represents the VSB, $[c_b]$ and $[k_b]$ are the distribution submatrix of the damping matrix $[C_b]$ and the spring stiffness matrix $[K_b]$ along the artificial boundary, respectively. The subscript "b" indicates an artificial boundary. E is the elastic modulus of the medium, G is the shear elastic modulus, r_b is the distance from the scattering source to the artificial boundary, and ρ is the density of the two-phase medium. The shear wave velocity V_s is similar to that of the single phase solid medium, i.e. $V_s = \sqrt{G/\rho}$.

4.4. The effect of absorption energy of VSB

The numerical model in Fig. 6 is still employed to calculate the dynamic response. The bottom surface and the four sides are bonded with the artificial VSB. The time interval takes to be 0.004s and the loading time 15s. For detailed implementation steps of SSOM with VSB, one can seek in Appendix II.

Under the two boundary conditions of VSB and the fixed boundary, the pore water pressure and the vertical displacement (in the Z-direction) cloud diagram after loading 15s are shown in Fig. 9 and Fig. 10, respectively.

Comparing Fig. 9 with Fig. 10, it can be seen that the pore water pressure and displacement distribution of the two boundary conditions are different. Under the VSB condition, the deformation is closer to reality due to the spring constraint imposed by the boundary, the boundary damping causes the pore water pressure to dissipate more quickly to the surrounding boundary, and the maximum pore pressure in the central region is only 0.01185 Pa. Under fixed boundary conditions, the displacement wave and the pressure wave are blocked by the interception boundary of the infinite domain and cannot be outwardly diffused. The deformation gradient is relatively large near the loading surface. Except for the ground permeable, the pore water pressure is difficult to diffuse in other directions.

To show the fluctuations in pore water pressure and displacement more clearly, the pore water pressure and displacement time history of

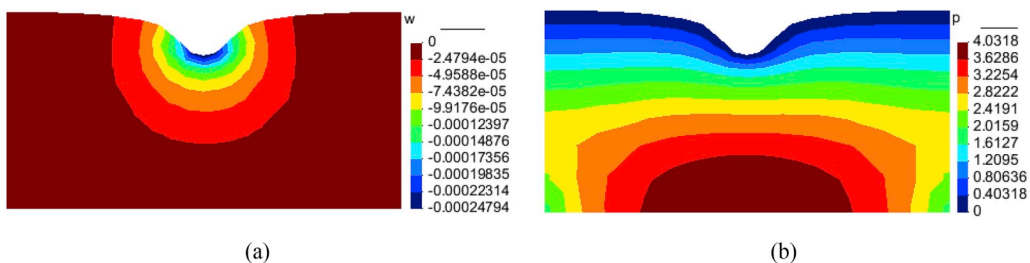


Fig. 10. The calculated results by SSOM with fixed boundary: The cloud diagram of (a) the vertical displacement (m) in the Z-direction, and (b) pore pressure (Pa) on the symmetrical section, respectively.

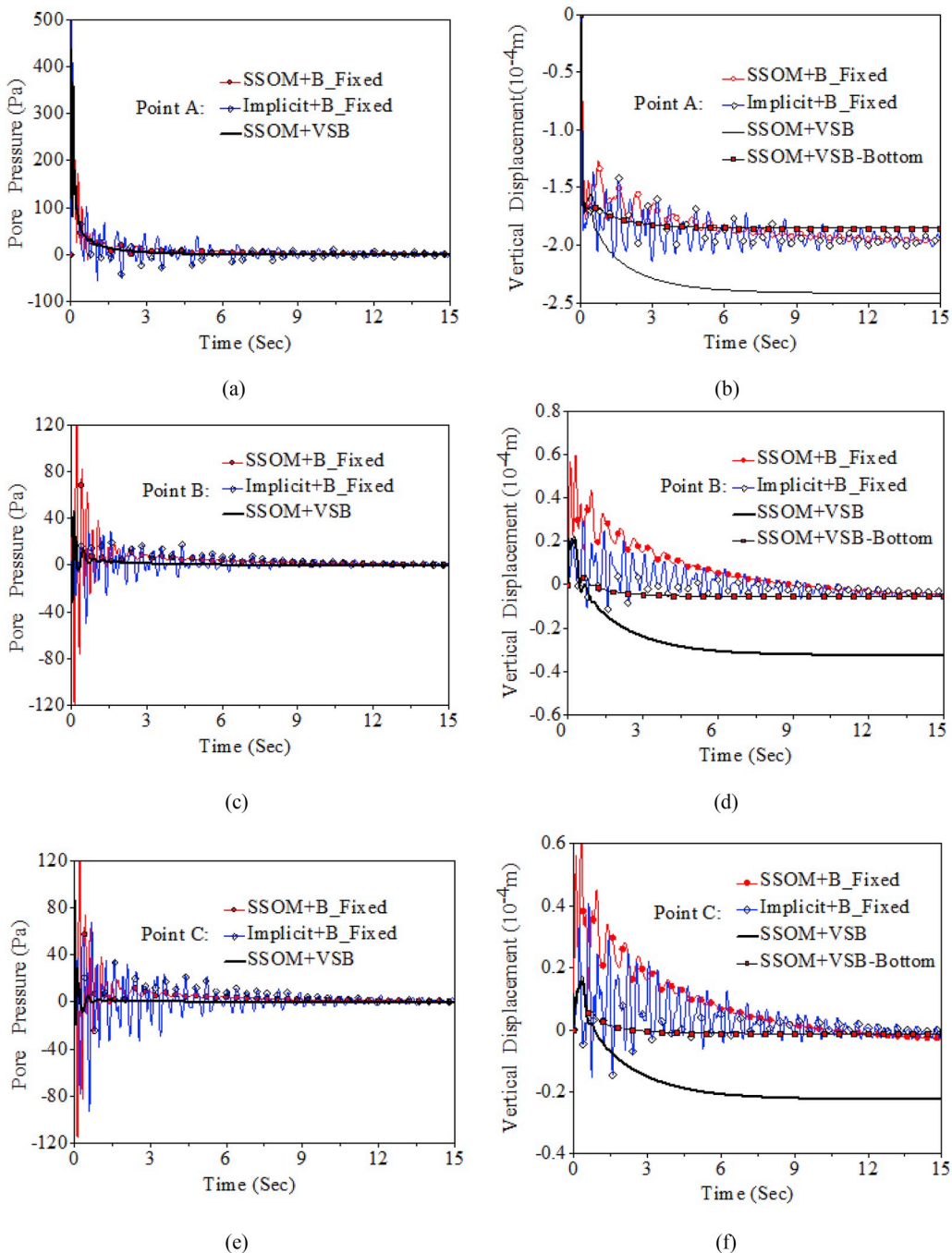


Fig. 11. Effect of absorption energy of VSB: Time histories of the pore pressure presented in the left column: (a) at point A, (c) at Point B, and (e) at Point C; Displacement responses presented in the right column: (b) at point A, (d) at Point B, and (f) at Point C.

Table 4
Calculation results of the pore water pressure by the different methods loading end to 15s.

Methods & cases	SSOM + B_Fixed (Pa)	Implicit + B_Fixed (Pa)	SSOM + VSB (Pa)
Point A	0.479	-1.286	0.004
Point B	0.483	1.252	0.001
Point C	0.471	1.557	0.000

Table 5
Calculation results of the displacements by the different methods loading end to 15s.

Methods & cases	SSOM + B_Fixed (mm)	Implicit + B_Fixed (mm)	SSOM + VSB (mm)	SSOM + VSB-Bottom (mm)
Point A	-1.963E-1	-1.940E-1	-2.416E-1	-1.855E-01
Point B	-4.347E-3	-3.786E-3	-3.241E-2	-5.470E-03
Point C	-2.801E-3	-1.367E-3	-2.239E-2	-1.300E-03

points A, B and C in Fig. 6 are given in Fig. 11 and compared with the corresponding calculation results with the fixed boundary in Section 3.3. It shows that both the pore water pressure (see Fig. 11 (a), (c) and (e)) and the vertical displacement (see Fig. 11(b), (d) and (f)) of the three representative points quickly tend to the stable solution after the initial fluctuation by using the VSB, while there are some fluctuations in the later stage when the boundary is fixed. Specially, at point B and point C near a fixed boundary, the pressure of pore water and displacement has a larger fluctuation about in the first 5 s, afterwards, the fluctuation amplitude becomes smaller and tends to be stable.

Actually, we can see that the pore water pressures tend to be consistent no matter what methods and boundary conditions we used. The residues of the pore water pressure in different situations at 15s (See Table 4) are negligible relative to the peak load (1000Pa).

For the displacement, the calculation results of both methods incline to be consistent with fixed boundary condition, but the displacements calculated by applying VSB become quite different (See Table 5). This is due to the deformation caused by distributed springs on the VSB (See Fig. 9(a)). After subtracting the displacements of corresponding points on the bottom boundary of Point A, B, C from their absolute displacements, the resulting relative displacements (SSOM + VSB-Bottom) are almost the same as the other calculation results. Moreover, one can also see that the rigid displacements of the boundary will not affect the results of pore water pressure and foundation stress, since the resulting pore water pressures are almost the same (See Fig. 11(a), (c), (e)).

According to the wave theory, the emission of pressure and displacement waves at a fixed boundary causes oscillation of the pressure of pore water and displacement. On the other hand, it can be seen that the viscoelasticity of VSB absorbs the energy of the outgoing wave. VSB model accurately simulates the damping effect of the far field ground. The numerical analysis of VSB and fixed boundary leads us to the conclusion that the proposed VSB model has a good absorption effect. Consequently, it is proved that SSOM combined with VSB model can

Appendix J. Supplementary data

Supplementary data to this article can be found online at <https://doi.org/10.1016/j.soildyn.2019.105803>.

Appendix I. Implicit scheme for dynamic consolidation equations

For the three-dimensional consolidation problem, denote by $D^{6 \times 6}$ the elastic matrix. Differential operator $L^{6 \times 3} \left(\frac{\partial}{\partial x_1}, \frac{\partial}{\partial x_2}, \frac{\partial}{\partial x_3} \right)$ and the related coefficient matrix are presented as

simulate the dynamic consolidation process of saturated porous semi-infinite foundation effectively and accurately.

5. Conclusions and remarks

In this paper, the splitting operator algorithm is investigated for solving differential equations with multiple physical variables. Five steps symmetrized splitting operator method for the dynamic consolidation equation of two-phase saturated medium $u-p$ is proposed. The splitting operator and variable decoupling are carried out to solve the second order explicit for the $u-p$ form of dynamic consolidation equations of the saturated porous medium. The numerical simulation of the displacement and pore water pressure diffusion process agree well with the theoretical results. Further numerical verification shows that the proposed SSOM has good precision, stability, and higher computational efficiency compared to implicit format calculations.

Numerical examples lead us to the conclusion that SSOM has a significant advantage in solving the longtime consolidation problems and the large-scale numerical simulation of dynamic consolidation. Combing with the artificial viscous-spring boundary, the seismic response of saturated porous soil structure and semi-infinite foundation system can be solved effectively and accurately.

Acknowledgments

The authors acknowledge financial supports from the National Key Research and Development Program of China, China (2017YFC0404906), the National Natural Science Foundation of China, China (Grant Nos.51679265, 51679264 and 51775523), IWHR Research & Development Support Program, China (EB0145B412016). The authors would like to thank Prof. Huai Zhang at University of Chinese Academy of Sciences for his constructive suggestions.

$$\mathbf{L} = \begin{bmatrix} \frac{\partial}{\partial x_1} & 0 & 0 \\ 0 & \frac{\partial}{\partial x_2} & 0 \\ 0 & 0 & \frac{\partial}{\partial x_3} \\ \frac{\partial}{\partial x_2} & \frac{\partial}{\partial x_1} & 0 \\ 0 & \frac{\partial}{\partial x_3} & \frac{\partial}{\partial x_2} \\ \frac{\partial}{\partial x_3} & 0 & \frac{\partial}{\partial x_1} \end{bmatrix}, \mathbf{L}^T = \begin{pmatrix} \frac{\partial}{\partial x_1} & 0 & 0 & \frac{\partial}{\partial x_2} & 0 & \frac{\partial}{\partial x_3} \\ 0 & \frac{\partial}{\partial x_2} & 0 & \frac{\partial}{\partial x_1} & \frac{\partial}{\partial x_3} & 0 \\ 0 & 0 & \frac{\partial}{\partial x_3} & 0 & \frac{\partial}{\partial x_2} & \frac{\partial}{\partial x_1} \end{pmatrix}, \mathbf{m}^T = [1 \ 1 \ 1 \ 0 \ 0 \ 0],$$

Denote the effective stress vectors and strain by

$$\boldsymbol{\sigma}'^T = [\sigma'_{xx} \ \sigma'_{yy} \ \sigma'_{zz} \ \tau'_{xy} \ \tau'_{xz} \ \tau'_{yz}], \boldsymbol{\varepsilon}^T = [\varepsilon_{xx} \ \varepsilon_{yy} \ \varepsilon_{zz} \ \varepsilon_{xy} \ \varepsilon_{xz} \ \varepsilon_{yz}]$$

where $\boldsymbol{\varepsilon} = \mathbf{L}\mathbf{u} = \begin{bmatrix} \frac{\partial}{\partial x_1} & 0 & 0 \\ 0 & \frac{\partial}{\partial x_2} & 0 \\ 0 & 0 & \frac{\partial}{\partial x_3} \\ \frac{\partial}{\partial x_2} & \frac{\partial}{\partial x_1} & 0 \\ 0 & \frac{\partial}{\partial x_3} & \frac{\partial}{\partial x_2} \\ \frac{\partial}{\partial x_3} & 0 & \frac{\partial}{\partial x_1} \end{bmatrix} \begin{Bmatrix} u \\ v \\ w \end{Bmatrix} = \begin{Bmatrix} \frac{\partial u}{\partial x_1} \\ \frac{\partial v}{\partial x_2} \\ \frac{\partial w}{\partial x_3} \\ \frac{\partial u}{\partial x_2} + \frac{\partial v}{\partial x_1} \\ \frac{\partial v}{\partial x_3} + \frac{\partial w}{\partial x_2} \\ \frac{\partial u}{\partial x_3} + \frac{\partial w}{\partial x_1} \end{Bmatrix}$.

Denote the volumetric strain of the solid skeleton by

$$\theta = \mathbf{m}^T \boldsymbol{\varepsilon} = \mathbf{m}^T \mathbf{L}\mathbf{u} = [1 \ 1 \ 1 \ 0 \ 0 \ 0] \begin{Bmatrix} \frac{\partial u}{\partial x_1} \\ \frac{\partial v}{\partial x_2} \\ \frac{\partial w}{\partial x_3} \\ \frac{\partial u}{\partial x_2} + \frac{\partial v}{\partial x_1} \\ \frac{\partial v}{\partial x_3} + \frac{\partial w}{\partial x_2} \\ \frac{\partial u}{\partial x_3} + \frac{\partial w}{\partial x_1} \end{Bmatrix} = \frac{\partial u}{\partial x_1} + \frac{\partial v}{\partial x_2} + \frac{\partial w}{\partial x_3}$$

$$\mathbf{L}^T \boldsymbol{\sigma}' = \begin{pmatrix} \frac{\partial}{\partial x} & 0 & 0 & \frac{\partial}{\partial y} & 0 & \frac{\partial}{\partial z} \\ 0 & \frac{\partial}{\partial y} & 0 & \frac{\partial}{\partial x} & \frac{\partial}{\partial z} & 0 \\ 0 & 0 & \frac{\partial}{\partial z} & 0 & \frac{\partial}{\partial y} & \frac{\partial}{\partial x} \end{pmatrix} \begin{pmatrix} \sigma'_{xx} \\ \sigma'_{yy} \\ \sigma'_{zz} \\ \tau'_{xy} \\ \tau'_{yz} \\ \tau'_{xz} \end{pmatrix} = \begin{pmatrix} \frac{\partial \sigma'_{xx}}{\partial x} + \frac{\partial \tau'_{xy}}{\partial y} + \frac{\partial \tau'_{xz}}{\partial z} \\ \frac{\partial \tau'_{xy}}{\partial x} + \frac{\partial \sigma'_{yy}}{\partial y} + \frac{\partial \tau'_{yz}}{\partial z} \\ \frac{\partial \tau'_{xz}}{\partial x} + \frac{\partial \tau'_{yz}}{\partial y} + \frac{\partial \sigma'_{zz}}{\partial z} \end{pmatrix}$$

Rewrite Eq. (2) as a vector form:

$$\begin{cases} \mathbf{L}^T (\boldsymbol{\sigma}' + \alpha \mathbf{m}p) + \rho \ddot{\mathbf{u}} = \rho \mathbf{b}, \\ \nabla^T k_f \nabla p + \alpha \mathbf{m}^T \mathbf{L} \dot{\mathbf{u}} - \frac{1}{Q} \dot{p} = 0 \end{cases} \tag{A1.1}$$

where $\boldsymbol{\sigma}' = \mathbf{D}\boldsymbol{\varepsilon} = \mathbf{D}\mathbf{L}\mathbf{u}$, u and p is presented by the interpolation function N_u and N_p , respectively. Then $\mathbf{u} = \mathbf{u}(t) = N_u \bar{\mathbf{u}} p = p(t) = N_p \bar{p}$, Eq. (A1.1) is discretized as

$$\begin{cases} \mathbf{M} \ddot{\mathbf{u}} + \mathbf{K}_d \dot{\mathbf{u}} + \mathbf{J} \bar{p} = \mathbf{F}_u \\ \mathbf{H} \bar{p} - \mathbf{S} \dot{\bar{p}} + \mathbf{J}^T \dot{\mathbf{u}} = \mathbf{F}_q \end{cases} \tag{A1.2}$$

where $M = \int_{\Omega} N_u^T \rho N_u d\Omega$, $K_d = \int_{\Omega} B^T \mathbf{D} B d\Omega$, $\mathbf{J} = \int_{\Omega} \alpha B^T \mathbf{m} N_p d\Omega$, $\mathbf{J}^T = \int_{\Omega} \alpha (\mathbf{m} N_p)^T B d\Omega$, $S = \int_{\Omega} N_p^T \frac{1}{Q} N_u d\Omega$, $\mathbf{F}_u = \int_{\Omega} N_u^T \rho \mathbf{b} d\Omega + \int_{\Gamma_c} N_u^T T d\Omega$, $\mathbf{F}_q = \int_{\Gamma_q} N_p^T \bar{q}_n d\Gamma$.

If the compressibility of the pore fluid (water) is neglected, the term $\dot{\bar{p}}$ is thus eliminated ($S = 0$). Afterwards, Eq. (A2) can be transformed to:

$$\begin{cases} \mathbf{M} \ddot{\mathbf{u}} + \mathbf{K}_d \dot{\mathbf{u}} + \mathbf{J} \bar{p} = \mathbf{F}_u \\ \mathbf{J}^T \dot{\mathbf{u}} + \mathbf{H} \bar{p} = \mathbf{F}_q \end{cases} \tag{A1.3}$$

The forward difference is adopted for the velocity vectors $\dot{\mathbf{u}}$ in the second equation above, while the Newmark's method is applied for the acceleration vectors $\ddot{\mathbf{u}}$ in the first equation. Eq. (A1.3) are then solved simultaneously. Note that the coefficient matrix of simultaneous Eq. (A1.3) is still asymmetrical. Therefore, an asymmetrical solver must be used to solve this equations.

Appendix II. Implementation steps of SSOM with VSB

Taking the boundary conditions into account, the detailed descriptions of each step to solve dynamic consolidation equation using SSOM (Eq. (8)) are displayed in an integral weak form as follows.

- 1) First give a time step Δt , initial values including $u_i(t=0)v_i(t=0)$, and $p(t=0)$;
- 2) Perform the following decomposition calculations in the time interval $(t_n, t_n + \Delta t)$:

- (1) Compute the subsystem $\varphi_1^u(\Delta t/2)$:

Let $u_i(t_n + \frac{\Delta t}{2}) = u_i(t_n)p(t_n + \frac{\Delta t}{2}) = p(t_n)$, obtain $v_i(t_n + \frac{\Delta t}{2})$ by Eq.(A2.1):

$$\int_{\Omega} \rho v_i \left(t_n + \frac{\Delta t}{2} \right) \delta u_i d\Omega = \int_{\Omega} \rho v_i(t_n) \delta u_i d\Omega - \frac{\Delta t}{2} \int_{\Omega} \sigma'_{ij}(t_n) \delta \varepsilon_{ij} d\Omega + \frac{\Delta t}{2} \int_{\Omega} \rho b_i \delta u_i d\Omega$$

$$+ \frac{\Delta t}{2} \int_{\Gamma_{\sigma}} T_i \delta u_i d\Gamma - \frac{\Delta t}{2} \int_{\Gamma_{vs}} [k_{bij}^m u_j(t_n) + c_{bij}^m \delta v_j(t_n)] \delta u_i d\Gamma_{vs}^m \quad (A2.1)$$

- (2) Compute the subsystem $\varphi_2^v(\Delta t/2)$:

Update $u_i(t_n + \frac{\Delta t}{2}) = u_i(t_n) + \frac{\Delta t}{2} v_i(t_n + \frac{\Delta t}{2})$, and yield $p(t_n + \frac{\Delta t}{2})$ by Eq. (A2.2):

$$\int_{\Omega} p \left(t_n + \frac{\Delta t}{2} \right) \delta p d\Omega = \int_{\Omega} p(t_n + \Delta t/2) \delta p d\Omega + \frac{\Delta t}{2} \alpha Q \int_{\Omega} \dot{\varepsilon}_{ii} \left(t_n + \frac{\Delta t}{2} \right) \delta p d\Omega \quad (A2.2)$$

- (3) Compute the subsystem $\varphi_3^p(\Delta t)$:

Obtain $v_i(t_n + \Delta t)$ by Eq. (A2.3), and $p(t_n + \Delta t)$ by Eq. (A2.4), respectively

$$\int_{\Omega} \rho v_i(t_n + \Delta t) \delta u_i d\Omega = \int_{\Omega} \rho v_i \left(t_n + \frac{\Delta t}{2} \right) \delta u_i d\Omega - \alpha \Delta t \int_{\Omega} p \left(t_n + \frac{\Delta t}{2} \right) \delta \varepsilon_{ii} d\Omega$$

$$- \alpha \Delta t \int_{\Gamma} p \left(t_n + \frac{\Delta t}{2} \right) n_i \delta u_i d\Gamma \quad (A2.3)$$

$$\int_{\Omega} p(t_n + \Delta t) \delta p d\Omega = \int_{\Omega} p \left(t_n + \frac{\Delta t}{2} \right) \delta p d\Omega - \Delta t k_f Q \int_{\Omega} p_i \delta p_i d\Omega - \Delta t Q \int_{\Gamma_q \cup \Gamma_{vs}} q_n \delta p d\Gamma \quad (A2.4)$$

On the artificial VSB, $q_n = \frac{\alpha k_f Q}{v_p^2} \dot{v}_n = \frac{\alpha k_f Q}{v_p^2} \left[\frac{v(t+\Delta t) - v(t)}{\Delta t} \right]$.

- (4) Compute the subsystem $\varphi_4^v(\Delta t/2)$:

Yield $u_i(t_n + \Delta t) = u_i(t_n + \frac{\Delta t}{2}) + \frac{\Delta t}{2} v_i(t_n + \Delta t)$, and update $p(t_n + \Delta t)$ by Eq. (A2.5):

$$\int_{\Omega} p(t_n + \Delta t) \delta p d\Omega = \int_{\Omega} p(t_n + \Delta t) \delta p d\Omega + \frac{\Delta t}{2} \alpha Q \int_{\Omega} \dot{\varepsilon}_{ii}(t_n + \Delta t) \delta p d\Omega \quad (A2.5)$$

- (5) Compute the subsystem $\varphi_5^u(\Delta t/2)$:

Update $v_i(t_n + \Delta t)$ by Eq. (A2.6):

$$\int_{\Omega} \rho v_i(t_n + \Delta t) \delta u_i d\Omega = \int_{\Omega} \rho v_i(t_n + \Delta t) \delta u_i d\Omega - \frac{\Delta t}{2} \int_{\Omega} \sigma'_{ij}(t_n + \Delta t) \delta \varepsilon_{ij} d\Omega + \frac{\Delta t}{2} \int_{\Omega} \rho b_i \delta u_i d\Omega$$

$$+ \frac{\Delta t}{2} \int_{\Gamma_{\sigma}} T_i \delta u_i d\Gamma - \frac{\Delta t}{2} \int_{\Gamma_{vs}} [k_{bij}^m u_j(t_n + \Delta t) + c_{bij}^m \delta v_j(t_n + \Delta t)] \delta u_i d\Gamma_{vs}^m \quad (A2.6)$$

- 3) Repeat Step 2), continue the computation of the next load step until the loading end.

References

- [1] Biot MA. Theory of propagation of elastic waves in a fluid-saturated porous solid. *J Acoust Soc Am* 1956;28:168–91.
- [2] Zienkiewicz OC, Shiomi T. Dynamic behaviour of saturated porous media; the generalized Biot formulation and its numerical solution. *Int J Numer Anal Methods Geomech* 1984;8:71–96.
- [3] López-Querol S, Fernández-Merodo JA, Mira P, Pastor M. Numerical modeling of dynamic consolidation on granular soils. *Int J Numer Anal Methods Geomech* 2008;32:1431–57.
- [4] Navas P, Yu RC, López-Querol S, Li B. Dynamic consolidation problems in saturated soils solved through u-w formulation in a LME mesh free framework. *Comput Geotech* 2016;79:55–72.
- [5] Zienkiewicz OC, Taylor RL. Coupled problems - a simple time-stepping procedure. *Commun Appl Numer Methods* 1985;1:233–9.

- [6] Felippa CA, Park KC. Staggered transient analysis procedures for coupled mechanical systems: Formulation. *J. Comp. Methods Appl. Mech. Eng.* 1980;24:61–111.
- [7] Park KC. Stabilization of partitioned solution procedure for pore fluid-soil interaction analysis. *Int J Numer Methods Eng* 1983;19(11):1669–73.
- [8] Zienkiewicz OC, Paul DK, Chan AHC. Unconditionally stable staggered solution procedure for soil-pore fluid interaction problems. *Int J Numer Methods Eng* 1988;26(5):1039–55.
- [9] Huang MS, Zienkiewicz OC. New unconditionally stable staggered solution procedures for coupled soil-pore fluid dynamic problems. *Int J Numer Methods Eng* 1998;43(6):1029–52.
- [10] Babuška I. Error bounds for finite element methods. *Numer Math* 1971;16:322–33.
- [11] Babuška I. The finite element method with Lagrange multipliers. *Numer Math* 1973;20:179–92.
- [12] Brezzi F. On the existence, uniqueness and approximation of saddle point problem from Lagrange multipliers. *Revue française d'automatique, informatique, recherche opérationnelle. Analyse numérique* 1974;8(2):129–51.
- [13] Zienkiewicz OC, Qu S, Taylor RL, Nakazawa S. The patch test for mixed formulation. *Int J Numer Methods Eng* 1986;23:1873–83.
- [14] Zienkiewicz OC, Huang MS, Wu J, Wu S. A new algorithm for coupled soil-pore fluid problem. *Shock Vib* 1993;1:3–14.
- [15] Taylor RL, Simo JC, Zienkiewicz OC, Chan ACH. The patch test - a condition for assessing FEM convergence. *Int J Numer Methods Eng* 1986;22:39–62.
- [16] Pastor M, Li T, Merodo JAF. Stabilized finite elements for cyclic soil dynamics problems near the undrained incompressible limit. *Soil Dyn Earthq Eng* 1997;16:161–71.
- [17] Huang MS, Wu SM, Zienkiewicz OC. Incompressible or nearly incompressible soil dynamic behaviour - a new staggered algorithm to circumvent restrictions of mixed formation. *Soil Dyn Earthq Eng* 2001;21(2):169–79.
- [18] Zienkiewicz OC, Wu J. Incompressibility without tears - how to avoid restrictions of mixed formulation. *Int J Numer Methods Eng* 1991;32:1189–203.
- [19] McLachlan RI. On the numerical integration of ordinary differential equations by symmetric composition methods. *SIAM J Sci Comput* 1995;16(1):151–68.
- [20] Bagrinovskii KA, Godunov SK. Difference schemes for multidimensional problems. *Dokl Akad Nauk SSSR* 1957;115:431–3.
- [21] Strang G. Accurate partial difference methods I: linear Cauchy problems. *Arch Ration Mech Anal* 1963;12(1):392–402.
- [22] Yasuo T. An economical explicit time integration scheme for A primitive model. *J Meteorol Soc Jpn* 1983;61(2):269–87.
- [23] Zeng Q, Yuan C. A split method to solve equations of weather prediction. *Kexue Tongbao (Foreign Lang Ed)* 1980;25(12):1005–9.
- [24] Zeng Q, Li R, Ji Z, et al. A numerical modeling for the monthly mean circulations in the South China Sea. *Sci Atmos Sin* 1989;13(2):127–38.
- [25] Karlsena KH, Liec KA, Natvigc JR, Nordhauga HF, Dahlea HK. Operator splitting methods for systems of convection-diffusion equations: nonlinear error mechanisms and correction strategies. *J Comput Phys* 2001;173(2):636–63.
- [26] Marinova RS, Christov CI, Marinov TT. A fully coupled solver for incompressible Navier-Stokes equations using operator splitting. *Int J Comput Fluid Dyn* 2003;17(5):371–85.
- [27] Çiçek Y, Tanoğlu G. Strang splitting method for Burgers-Huxley equation. *Appl Math Comput* 2016;276:454–67.
- [28] Gücüyenlen N. Strang splitting method to Benjamin-Bona-Mahony type equations: analysis and application. *J Comput Appl Math* 2017;318:616–23.
- [29] Xiao J, Qin H, Liu J, He Y, Zhang R, Sun Y. Explicit high-order non-canonical symplectic particle-in-cell algorithms for Vlasov-Maxwell systems. *Phys Plasmas* 2015;22:112504.
- [30] He Y, Sun Y, Qin H, Liu J. Hamiltonian particle-in-cell methods for Vlasov-Maxwell equations. *Phys Plasmas* 2016;23(9). 2669-58.
- [31] Wang B, Ji Z. An improved splitting method. *Adv Atmos Sci* 1993;10(4):447–52.
- [32] Einkemmer L, Ostermann A. An almost symmetric Strang splitting scheme for nonlinear evolution equations. *Comput Math Appl* 2014;67(12):2144–57.
- [33] Liao ZP. Introduction to wave motion theories in engineering. second ed. Beijing: China Science Press; 2002. p. 156–63.
- [34] Lysmer J, Kuhlemeyer RL. Finite dynamic model for infinite media. *J Eng Mech Div* 1969;95(4):859–78.
- [35] Deeks AJ, Randolph MF. Axisymmetric time-domain transmitting boundary. *J Eng Mech* 1994;120(1):25–42.
- [36] Liu J, Wang Z, Du X, Du Y. Three dimensional visco-elastic artificial boundaries in time domain for wave motion problems. *Chin. Eng. Mech.* 2005;22(6):46–51.
- [37] Ma H, Wang L, Chen H. Principle of virtual displacements of viscous-spring artificial boundaries. *Chin. Eng. Mech.* 2013;30(1):168–74.
- [38] Wolf JP, Song C. Finite-element modeling of unbounded media. New York: Wiley; 1996.
- [39] Bazylar MH, Song C. Analysis of transient wave scattering and its applications to site response analysis using the scaled boundary finite-element method. *Soil Dyn Earthq Eng* 2017;98:191–205.
- [40] Lu S, Liu J, Lin G. High performance of the scaled boundary finite element method applied to the inclined soil field in time domain. *Eng Anal Bound Elem* 2015;56:1–19.
- [41] Modaressi H, Benzenati I. An absorbing boundary element for dynamic analysis of two-phase media. Earthquake engineering, tenth world conference. Madrid, Spain. Rotterdam: Balkema; 1992. p. 1157–61.
- [42] Akiyoshi T, Fuchida K, Fang HL. Absorbing boundary conditions for dynamic analysis of fluid-saturated porous media. *Soil Dyn Earthq Eng* 1994;13:387–97.
- [43] Liu G, Song E. Visco-elastic transmitting boundary analysis of infinite saturated soil foundation. *Chin J Geotech Eng* 2006;28(12):2128–33.